A Multilevel Inverter Topology for Inductively Coupled Power Transfer

John I. Rodriguez, *Member, IEEE*, and Steven B. Leeb, *Senior Member, IEEE*

***Abstract*—This paper describes a multilevel inverter that can synthesize quantized approximations of arbitrary ac waveforms. This converter could be used to deliver power over multiple frequencies simultaneously. Unlike traditional multilevel inverters, this topology does not require an external voltage balancing circuit, a complicated control scheme, or isolated dc sources to maintain its voltage levels while delivering sustained real power. In this paper, we use this circuit for heating frequency selectable induction targets designed to stimulate temperature sensitive polymer gel actuators. For this application our multilevel inverter offers higher efficiency than a pulse width modulated full-bridge inverter (a more conventional power supply solution) at comparable levels of total harmonic distortion.**

***Index Terms*—Dynamic vibration absorber, induction heating, Marx generator, multilevel inverters.**

I. Background

WE ARE developing an adaptive vibration damper capable of adjusting its natural frequency to improve damping over a range of vibration frequencies. This damper is an auxiliary spring-mass system and is sometimes called a dynamic vibration absorber (DVA) [1]. When a DVA is mechanically coupled to a vibrating structure such as an automobile engine, or a building, it creates a higher order mechanical system with at least one resonance and one anti-resonance. At the DVA's natural frequency, the total system experiences an anti-resonance where the mass of the DVA and the mass of the vibrating structure move in counterpoise. The mass of the primary mechanical structure remains relatively stationary while the DVA oscillates as a result of "absorbing" the disturbing vibration.

Typically, a DVA is designed to provide maximum damping at its fixed natural frequency. A more sophisticated DVA can adjust its natural frequency by varying its spring constant with a magnetic actuator, a responsive material, or some other scheme [2]. Because the DVA concept applies equally well to both linear and rotational systems, a controllable moment of inertia can also be exploited. Fig. 1(a) shows a simplified model of a rotational DVA with an adjustable moment of inertia. A variable inertia, J_2, is created using a cylindrical container filled with a gel fluid. This fluid consists of temperature sensitive polymer gel beads suspended in a solvent. Below a certain temperature

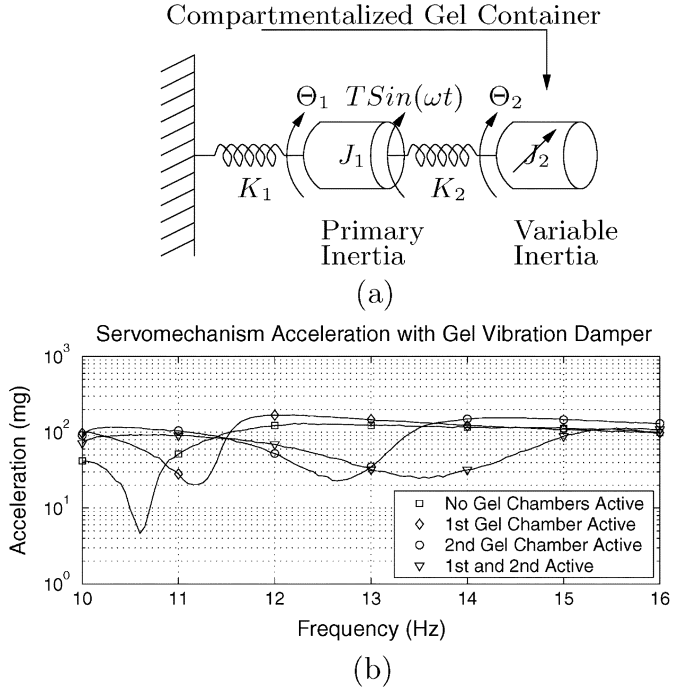

Fig. 1. Torsional gel damper. (a) Simplified model. (b) Acceleration response versus frequency of the primary inertia J_1.

the gel beads swell, absorbing the surrounding solvent into the polymer matrix (like a sponge). When this happens, the gel beads pack tightly in the container, adding significantly to the container's effective moment of inertia. At higher temperatures the polymer network shrinks, allowing the solvent to flow freely. This effectively decouples the gel-solvent mass and lowers the apparent rotational inertia J_2. By subdividing the container into n compartments of varying gel mass, 2^n anti-resonant states are made possible depending on which compartments are heated. Fig. 1(b) shows peak damping at four different vibration frequencies created by a two-compartment gel DVA prototype.

II. Frequency Selectable Induction Heating Targets

Heating the polymer gels is complicated because each compartment is sealed (to prevent the escape of solvent). Approaches that use external control wires for heating would add unwanted damping, thereby reducing the vibration absorber's effectiveness. Furthermore, it is economically and mechanically advantageous to keep the packaging of each compartment simple. Heating schemes that require contact with a gel compartment are therefore undesirable. Induction heating the gel compartments delivers heat without physical contact, a distinct advantage in this

Manuscript received June 28, 2004; revised January 11, 2006. This work was supported by the National Science Foundation through a MRSEC Grant, a Grainger Foundation Grant, and support from the Ford Motor Company. Recommended by Associate Editor J. D. van Wyk.

J. I. Rodriguez is with Talking Lights, LLC, Brighton, MA 02135 USA (e-mail: jirodrig@mit.edu).

S. B. Leeb is with the Laboratory for Electromagnetic and Electronic Systems, Massachusetts Institute of Technology, Cambridge, MA 02139-4307 USA.

Digital Object Identifier 10.1109/TPEL.2006.882965

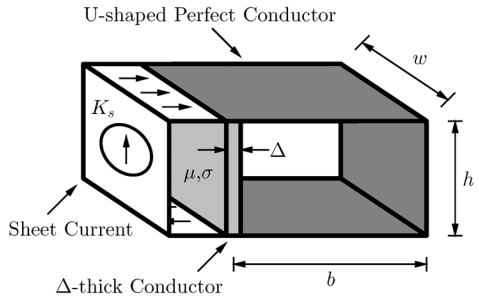

Fig. 2. Perfectly conducting U-shaped conductor which is bridged by a Δ-thick conductor and driven by a sinusoidal current sheet can be used to illustrate how a thin-walled conductor can act as a magnetic shield or induction heating target.

and other (including medical) applications. In the multicompartment DVA, the induction heating system must be capable of selectively heating any combination of gel compartments.

In our prototype, each gel compartment contains an induction target that heats preferentially at one frequency with respect to the other targets. A single converter that can drive a sum of sinewaves across a single "primary-side" induction coil has the potential to simultaneously heat the desired combination of induction targets. The frequency selective targets used in our DVA do not require a separate induction coil for each target, unlike other multiload/single converter induction heating systems [3].

The term "induction heating" refers to situations where a time-varying magnetic field gives rise to eddy currents in a conductor and therefore ohmic dissipation. In a typical case these eddy currents crowd near the conductor's surface with a profile that decays exponentially into the conductor at a rate determined by its skin depth δ. These eddy currents terminate the time-varying magnetic field, permitting the conductor to act as a shield. If additional shielding or heating is needed, the conductor's thickness can be increased until the magnetic field is completely terminated. Perhaps counter-intuitively, a thin-walled conductor whose thickness is small compared to its skin depth δ can also act as a good magnetic shield or induction target. This phenomenon is explained in [4] and summarized with the help of Fig. 2.

Here, a perfectly conducting U-shaped conductor is driven by a sheet current $K_s = K_o \sin(\omega t)$, where it is assumed that the conductor's width w is great enough to eliminate variation of the field solution along this axis. A Δ-thick conductor bridges the open end of the U-shaped conductor. When the Δ-thick conductor is such that $\Delta \ll \delta$, it can be thought of as forming a current divider with the U-shaped perfect conductor. If we define the conductance per unit width $G = \sigma\Delta/h$, and the inductance times a unit width $L = \mu bh$, for this structure, the complex amplitude of the current flowing through the Δ-thick conductor is

$$K_\Delta = \frac{j\omega LG}{1 + j\omega LG} K_o. \tag{1}$$

Essentially, the magnetic energy stored in the region to the right of the Δ-thick conductor in Fig. 2 is modeled as energy stored in a lumped inductor. As the drive frequency increases, the effective impedance of this inductance increases also, forcing a greater fraction of the drive current into the resistive sheet. This frequency response is analogous to the current that flows through the resistive leg of a parallel L–R circuit when

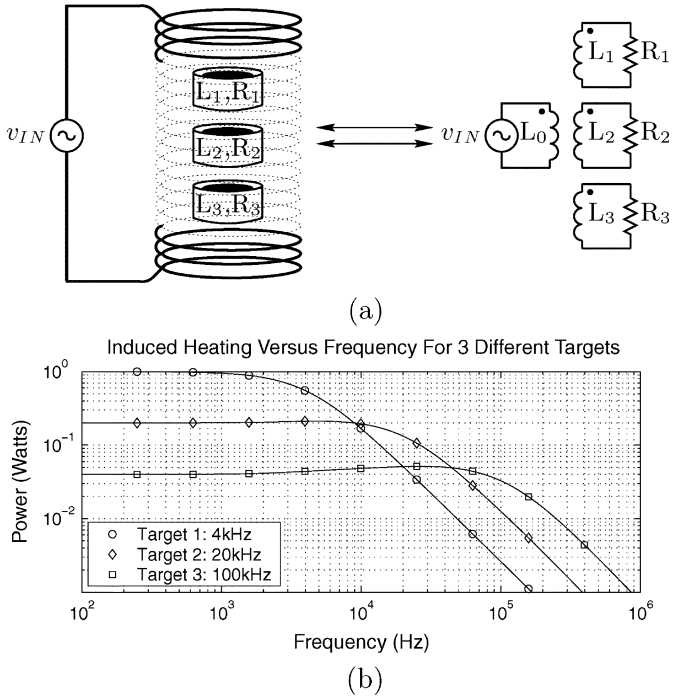

Fig. 3. Multiple target induction heating scheme: (a) circuit model and (b) power curves versus frequency for three different induction heating targets.

driven by a sinusoidal current source input. Consequently, the Δ-thick conductor can be modeled as a parallel L–R circuit providing that $\Delta \ll \delta$ over the frequencies of interest. Unlike the thick conductor case, the shielding (or heating) strategy for the thin-conductor is to increase the length, b, of the U-shaped conductor, thereby increasing its inductance and shunting more current through the Δ-thick conductor for a given frequency.

If thin-walled conductors are used as induction targets, a preferential heating scheme can be devised by designing the targets with similar self-inductances but different resistances. Consider for example, three shorted, single-turn inductors each with a different resistance, all of which are coupled to a single "primary" induction coil driven by a sinusoidally varying voltage as illustrated in Fig. 3(a). Assuming that the cross-coupling between targets is negligible, it can be shown that the time-averaged power dissipated in target n (1, 2, or 3) when evaluated at that target's characteristic frequency (in Hertz)

$$f_n = \frac{\omega_n}{2\pi} = \frac{R_n}{2\pi L_n} \tag{2}$$

is given by

$$\langle P_n(f_n) \rangle = \frac{\pi}{2} L_0 (K_n \cdot I_o)^2 f_n. \tag{3}$$

The term I_o is the amplitude of the primary side current, while K_n represents the coupling coefficient between the primary coil and target n, and is defined using the mutual inductance L_{0n}, between L_0 and L_n

$$K_n = \frac{L_{0n}}{\sqrt{L_0 L_n}}. \tag{4}$$

If the resistance between two targets differs by a factor of α, i.e., $R_{n+1} = \alpha R_n$, it can be shown that the time-averaged power

dissipated in R_n when driven at its characteristic frequency is [5], [6]

$$\langle P_n(f_n)\rangle = \frac{\alpha^2+1}{2\alpha}\left(\frac{K_n}{K_{n+1}}\right)^2 \langle P_{n+1}(f_n)\rangle. \quad (5)$$

We will consider a three target system with a separation factor $\alpha = 5$. If a coupling coefficient, $K_n = 0.3$, between each target and primary coil is assumed, power delivered as a function of frequency is given by the curves in Fig. 3(b). Here, the associated target frequencies have been chosen as 4, 20, and 100 kHz. This plot shows that a target driven at its characteristic frequency heats at least 2.6× more than the remaining targets.

Fig. 3(b) also shows that for a voltage drive, the power dissipated in a target falls with increasing frequency. This decrease is the result of the induction coil's increasing impedance at these frequencies, hence a greater drive voltage is needed here to generate the same amplitude H-field within the induction coil. The primary-side power supply must be able to produce sinewaves at the desired frequencies with enough spectral purity to prevent unwanted heating in the remaining induction targets. If the drive waveform is a sum of sinewaves chosen from combinations of the three characteristic frequencies any combination of compartments can be heated simultaneously. A power supply that can deliver power concurrently at the required frequencies is the subject of the next section.

III. "Marx" Multilevel Inverter

A. Introduction

Multilevel converters have drawn attention for approximating sinewaves. A multilevel inverter is capable of generating M voltage levels where M is a number greater than two. Often these levels are derived from a voltage source using a capacitor voltage divider with multiple taps. The three most common multilevel converter topologies include the diode-clamped, capacitor-clamped and cascade-inverters with separate dc sources [7]. Unfortunately, to create three or more levels the first two topologies suffer from a significant capacitor voltage balancing problem when delivering real power. In the case of a three-level converter it is possible to maintain the dc-link potential with proper control. Beyond three levels, all of these multilevel converters require separate, isolated dc sources or a complicated voltage balancing circuit for active power transfer. As a result, multilevel converters have found limited application, notably as reactive power compensators. Recently, a generalized multilevel inverter topology with self-voltage balancing was proposed [8] that overcomes the limitations of the three major topologies for levels, M, greater than three. A drawback of this topology is that the number of active switching devices grows quadratically with the number of levels. The generalized topology is useful for inferring other possible multilevel inverters that are less part intensive—one such topology is presented here.

B. Principle of Operation

The proposed multilevel topology is based on a high voltage pulse circuit, known as a Marx generator (Erwin Marx, 1924). The basic idea behind the Marx generator is that it can produce a high voltage pulse by charging a bank of capacitors in parallel and discharging them in series. Connecting the capacitors in series is accomplished by a switching network originally comprised of spark gaps or avalanche type devices. When the first gap is triggered it sets into motion a cascade effect whereby each successive gap "fires" and all the capacitors are serially discharged. If these spark gaps are replaced by controllable switching devices it becomes possible to control the number of capacitors that are serially connected to the load. The result is a multilevel topology that generates required voltage levels by multiplying the dc bus voltage as opposed to dividing it down. Because the underlying principle behind this inverter is similar to the Marx generator, we will refer to this topology as the "Marx" multilevel inverter. Fig. 4 shows an example of a single phase, $M = 4$, Marx multilevel inverter.

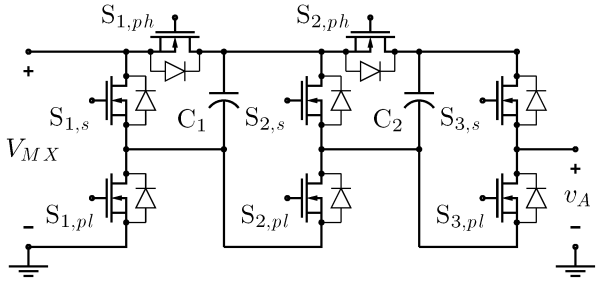

Fig. 4. Single-phase, four-level Marx inverter.

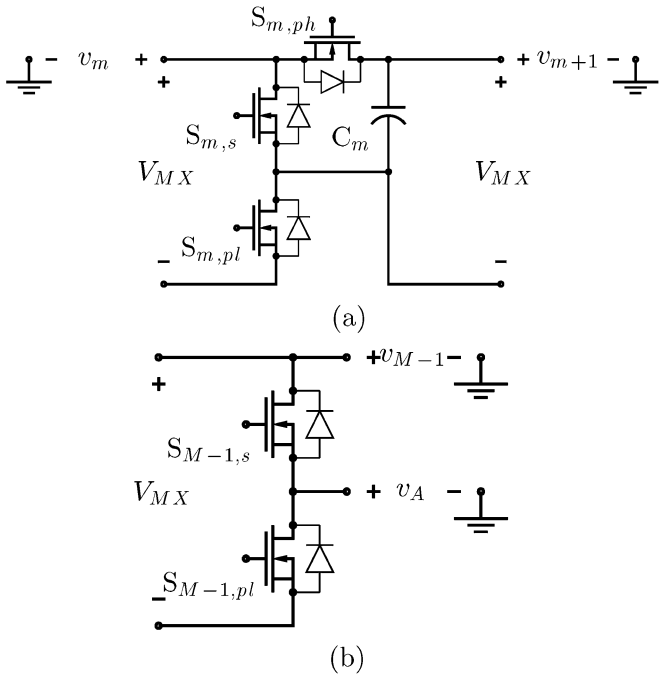

Fig. 5. Single phase, Marx inverter decomposition: (a) basic Marx cell. (mth stage shown) and (b) half-bridge inverter (Mth and final Marx stage).

An M-level Marx inverter can be decomposed into a cascade of M-2 Marx cells and one half-bridge inverter. The operation of this inverter can be understood by examining the basic Marx cell shown in Fig. 5(a). The mth Marx cell is composed of a capacitor, C_m, and three switches which serve to either parallel (via $S_{m,\mathrm{pl}}$, $S_{m,\mathrm{ph}}$) the capacitor with the (m-1)th cell preceding it or to connect it in series (via $S_{m,s}$). When paralleled the output voltage of the mth cell is

$$v_{m+1} = v_m, \quad (6)$$

or when connected in series

$$v_{m+1} = v_m + V_{\mathrm{MX}} \quad (7)$$

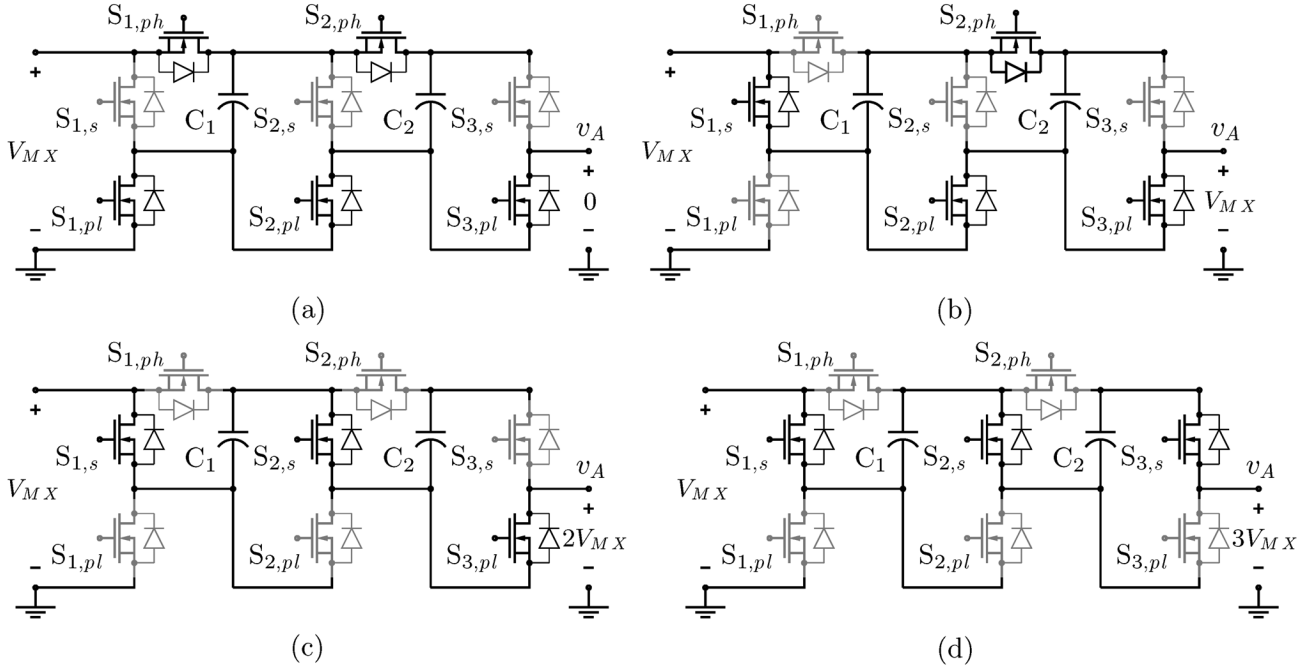

Fig. 6. One implementation of the switching states for a single-phase, four-level Marx inverter. Switches that are on are shown in black, while switches that are off are shown in gray. It is assumed that all of the capacitors in this example have been charged to $\mathrm{V_{MX}}$. Four states are shown. (a) $v_A = 0$: $S_{1,\mathrm{pl}}$, $S_{1,\mathrm{ph}}$, $S_{2,\mathrm{pl}}$, $S_{2,\mathrm{ph}}$, $S_{3,\mathrm{pl}}$ are on, $S_{1,s}$, $S_{2,s}$, $S_{3,s}$ are off. C_1, C_2, and the V_{MX} input are in parallel. The output is connected to ground. (b) $v_A = V_{\mathrm{MX}}$: $S_{1,s}$, $S_{2,\mathrm{pl}}$, $S_{2,\mathrm{ph}}$, $S_{3,\mathrm{pl}}$ are on, $S_{1,\mathrm{pl}}$, $S_{1,\mathrm{ph}}$, $S_{2,s}$, $S_{3,s}$ are off. C_1, C_2 are in parallel. The output is connected to the V_{MX} input. (c) $v_A = 2V_{\mathrm{MX}}$: $S_{1,s}$, $S_{2,s}$, $S_{3,\mathrm{pl}}$ are on, $S_{1,\mathrm{pl}}$,$S_{1,\mathrm{ph}}$, $S_{2,\mathrm{pl}}$, $S_{2,\mathrm{ph}}$, $S_{3,s}$ are off. The output is connected in series with C_1 and the V_{MX} input. (d) $v_A = 3V_{\mathrm{MX}}$: $S_{1,s}$, $S_{2,s}$, $S_{3,s}$ are on, $S_{1,\mathrm{pl}}$, $S_{1,\mathrm{ph}}$, $S_{2,\mathrm{pl}}$, $S_{2,\mathrm{ph}}$, $S_{3,\mathrm{pl}}$ are off. The output is connected in series with C_1, C_2 and the V_{MX} input.

where it has been assumed that C_m has been charged to V_{MX}. By definition $v_1 = V_{\mathrm{MX}}$ and is provided by a dc voltage source. A cascade of M-2 Marx cells can be used to generate M-1 levels above ground, while the final stage shown in Fig. 5(b) can be used to either select one of these levels

$$v_A = v_{M-1} \tag{8}$$

or alternatively to select ground when all of the capacitors are in parallel

$$v_A = v_{M-1} - V_{\mathrm{MX}} = 0. \tag{9}$$

In general an M-level Marx inverter has 2^{M-1} possible switching states. Therefore, there are redundant states for some of the intermediate voltage levels. In the case of certain multilevel inverters, such as the capacitor-clamped topology, redundant switching states maybe useful for capacitor voltage balancing. Because the capacitor voltages of a Marx inverter are equalized to the bus voltage whenever all the capacitors are paralleled, redundant states need not be used. Instead, it is easier to use a set of states that simplifies the overall control. One scheme to do this is to stack the capacitors sequentially by starting from the source side. The switching states for this approach are shown in Table I. Alternatively, Fig. 6 illustrates each of these four switching patterns, depicting on-switches in black and off-switches in gray.

TABLE I
SWITCHING STATES FOR A SINGLE-PHASE, FOUR-LEVEL MARX INVERTER

$\mathbf{v_A}$	$\mathbf{S_{1,p}}$	$\mathbf{S_{2,p}}$	$\mathbf{S_{3,p}}$	$\mathbf{S_{1,s}}$	$\mathbf{S_{2,s}}$	$\mathbf{S_{3,s}}$
0	1	1	1	0	0	0
V_{MX}	0	1	1	1	0	0
$2V_{MX}$	0	0	1	1	1	0
$3V_{MX}$	0	0	0	1	1	1

C. Control and Modulation Strategy

Most control and modulation strategies for multilevel inverters are meant for synthesizing sinewaves at low frequencies for utility or industrial applications. In general these approaches fall into two categories [9].

- High switching frequency PWM techniques.
- Fundamental switching frequency techniques.

Two high frequency PWM methods, the classic sinusoidal PWM method and the space-vector PWM approach, are well-suited to low frequency sine generation. These schemes suffer from significant switching losses as well as switching speed limitations when trying to synthesize sinewaves in the 100–300 kHz range or higher. For high frequencies, fundamental switching frequency strategies can be advantageous, generally requiring fewer switching transitions to produce a sinusoidal approximation. A conventional six-pulse sinewave drive is a familiar example of a fundamental switching frequency technique. Example fundamental switch frequency strategies include the selective harmonic elimination approach [10] and the space-vector control technique [11].

We are examining a different fundamental switching frequency strategy—using two Marx inverters to create a circuit that behaves like a symmetric uniform quantizer. In the same

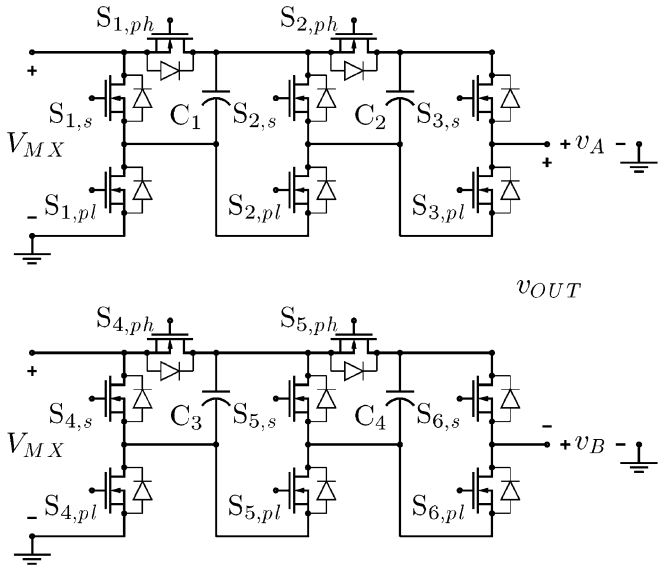

Fig. 7. Two $M = 4$, single phase Marx inverters can be be used to produce seven voltage levels differentially.

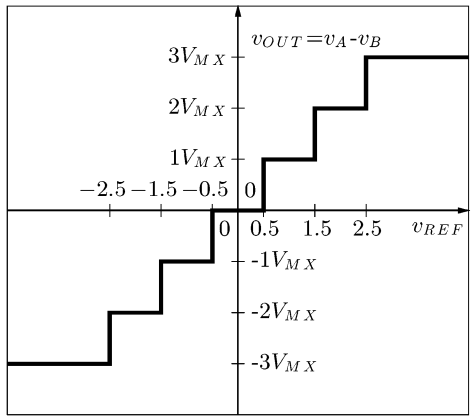

Fig. 8. Seven-level symmetric uniform mid-tread quantizer can be implemented with two $M = 4$, single phase Marx inverters and proper control.

way that two half-bridge inverters can be used to drive a load differentially by forming a full-bridge, two Marx inverters can also form a multilevel "full-bridge." Fig. 7 shows two $M = 4$, single phase Marx inverters that have been combined to drive a load differentially. This two-phase configuration can impress pure ac waveforms across a load assuming the load can be floated with respect to ground.

This control strategy can be implemented with a minimal amount of analog hardware, is simple to understand, and can be used to approximate more complicated ac waveforms (such as a sum of three sinewaves). This makes the Marx inverter suitable for driving multiple targets in our induction heating example. Hardware implementation consists of a bank of comparators that converts a reference waveform into a simple thermometer code, similar to those used in flash analog-to-digital converters. The output is then decoded (with an appropriate amount of inserted dead-time) to provide the correct gate drive logic for two $M = 4$, single-phase Marx inverters operated differentially. This hardware was used to implement a seven-level, symmetric uniform mid-tread quantizer whose transfer characteristic is shown in Fig. 8.

Fig. 9 is a collection of sample waveforms generated by a 1-kW prototype two-phase Marx inverter functioning as a seven-level quantizer. Two $M = 4$ phase legs are used to drive either a 200-μH air coil inductor Fig. 9(a)–(c) or a 100-Ω resistor Fig. 9(d) differentially. Each snapshot shows three waveforms which correspond (from top to bottom) to the input reference waveform, a multilevel approximation and the current drawn from the converter. As seen in these various scope plots, the Marx inverter can drive a variety of ac waveforms across an inductive load, and/or deliver real power while still maintaining appropriate voltage levels.

IV. Performance Comparison: PWM Full-Bridge VSI Versus Quantized Marx VSI

The simple full-bridge inverter has long been used to synthesize power-level sinewaves via pulse width modulation (PWM). The PWM full-bridge inverter was also considered as a power supply for the DVA induction heating targets. In comparison to the full-bridge the Marx inverter is a component-intensive circuit. The decision to choose the Marx inverter should therefore be justified on the basis of performance versus economic tradeoff. Although both converters can produce a sums of sinewaves we shall limit our analysis to single frequencies as a starting point for comparison. The two topologies will be evaluated using the following benchmarks.

1) The spectral purity of the generated output.
2) The converter's efficiency.

The first benchmark is measured by examining the THD present in the load current

$$\mathrm{THD} = \sqrt{\frac{I_{\mathrm{rms}}^2 - I_{\mathrm{rms},1}^2}{I_{\mathrm{rms},1}^2}} \tag{10}$$

where I_{rms} is the rms value of the load current and $I_{\mathrm{rms},1}$ is the rms value of the load current's fundamental component. The PWM full-bridge VSI, shown in Fig. 10, is a prime candidate for comparison against the quantized Marx inverter because of its popularity and simplicity. There are also a number of PWM strategies that could be used for comparison and include, but are not necessarily limited to, the naturally sampled, symmetric and asymmetric regular sampled schemes [12]. The naturally sampled strategy is the traditional analog scheme that determines the switching instances by comparing a sine reference against a high frequency triangle waveform. The other two schemes are digital approaches. In this paper we confine our comparison to the naturally sampled case since the proposed control for the Marx inverter is also analog. While there are a number of digital implementations that would allow for selective harmonic cancellation and hence improved performance in either type of converter, the analysis in this paper is still a fair starting point for comparison.

Depending on the implementation, a full-bridge can be made to produce either a bipolar or unipolar naturally sampled PWM waveform [13]. The unipolar pattern differs from the bipolar because it uses a 180° phase-shifted version of the reference sine for determining the switching instants of the second phase leg. For clarity, Fig. 11 shows an example of a naturally sampled unipolar PWM scheme where the modulation frequency has been arbitrarily chosen to be seven times (M_f =7) faster

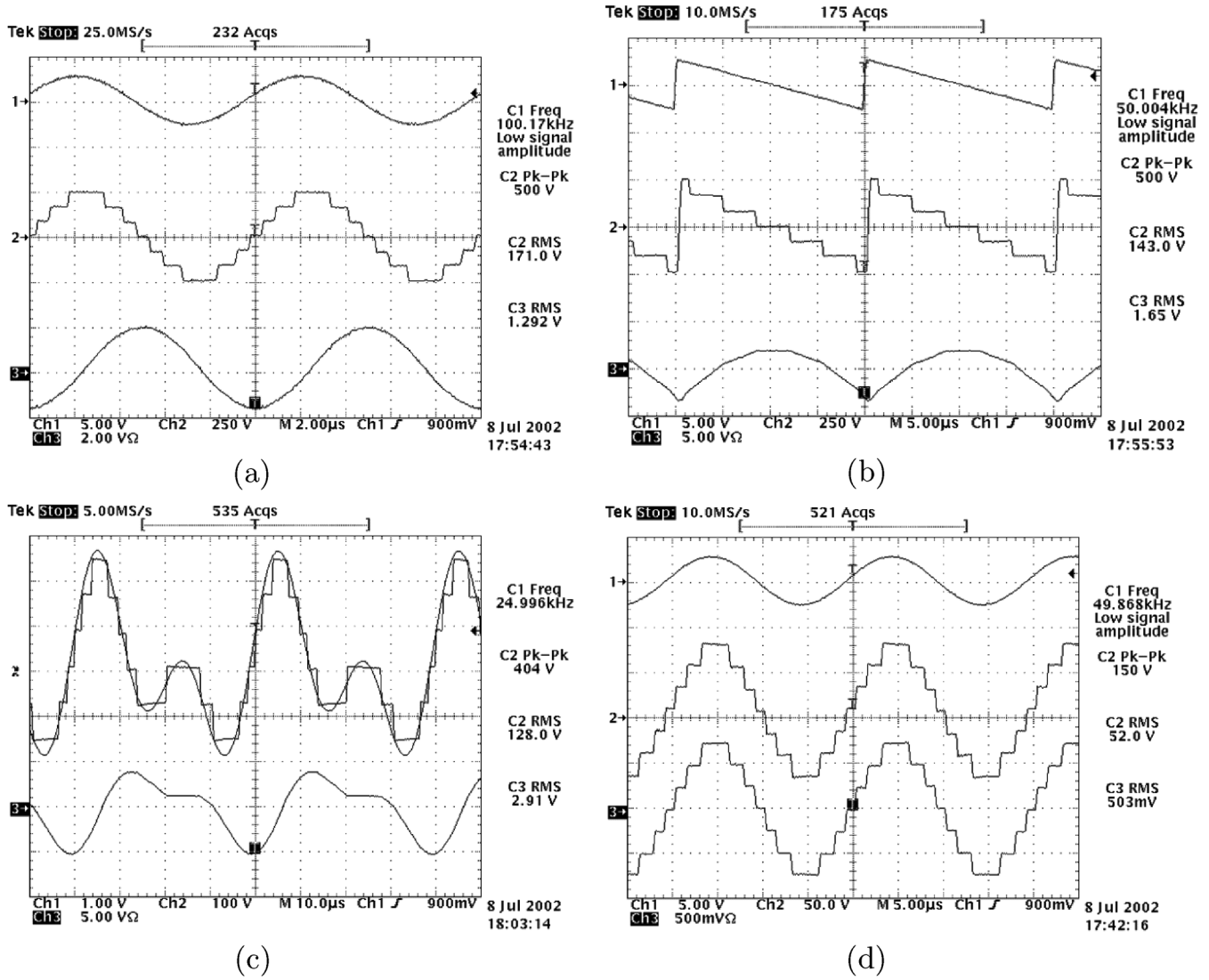

Fig. 9. Sample Marx inverter waveforms. Channels 1, 2, and 3 are the reference waveform, Marx output voltage and load current, respectively. For scaling purposes the measurements on channel 3 are consistent with 1 VΩy = 1 A. Four different reference waveform and load configurations are shown: (a) 100-kHz sinewave, 200-μH air core inductor, (b) 50-kHz sawtooth, 200-μH air core inductor, (c) sum of sinewaves (25 kHz, 50 kHz), 200-μH air core inductor, and (d) 50-kHz sinewave, 100-Ω resistor.

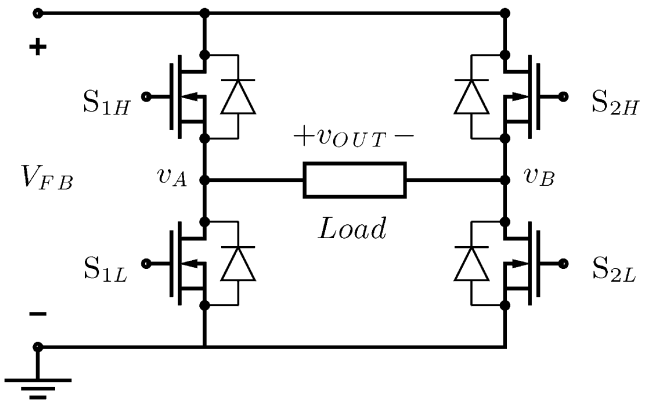

Fig. 10. Full-bridge inverter is often used for synthesizing power-level sinewaves.

than the carrier frequency. The unipolar pattern minimizes low frequency harmonic content for the full-bridge PWM inverter, and will be used here as a standard for comparison.

A. THD Comparison

In the absence of filtering, a sinewave that is generated by the quantizer in Fig. 8 will generally have less THD than a unipolar PWM waveform. This is not surprising, because PWM relies heavily on averaging to achieve a specific amplitude due to the relatively limited number of voltage levels a full-bridge can provide, i.e., three. The THD of the output voltage for both converters was computed using MATLAB over a normalized output range and is shown in Fig. 12(a). The results of the two-phase Marx inverter functioning as a seven-level symmetric uniform quantizer shows that its THD varies from about 86.5% to 12.5% over the output range. Alongside these results are those of the full-bridge PWM inverter for three different frequency modulation ratios: $M_f = 3$, 5, and 10. These plots show that the PWM distortion is roughly three to five times worse depending on the amplitude of the output and only improves marginally as the modulation ratio is increased from three to ten.

Ultimately, our goal is to drive a collection of induction targets, each at its own respective $R/(2\pi L)$ frequency with a low

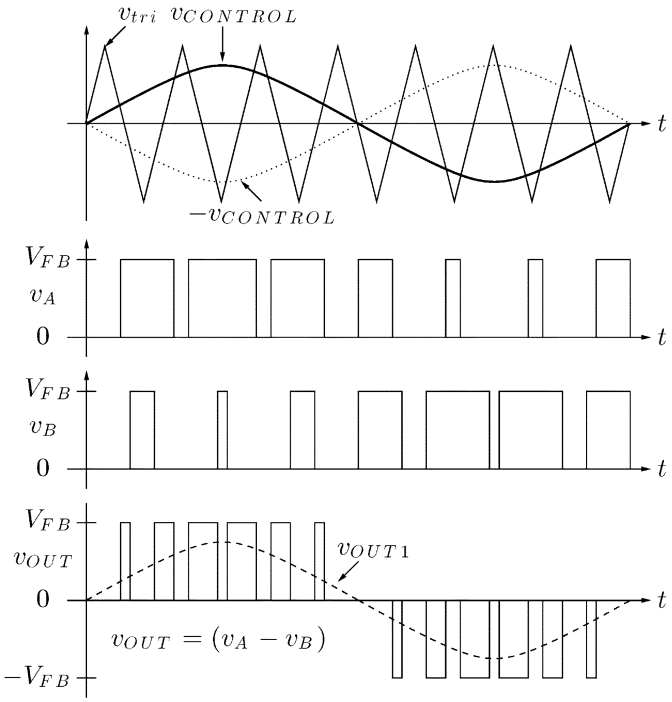

Fig. 11. Unipolar switching scheme with a frequency modulation ratio, $M_f = 7$.

distortion sinewave. In this application, the induction coil and targets form a low-pass filter whose effect must be considered when comparing the THD for both circuits. As a result, we will now focus on the THD associated with the load current which reflects this filtering. Before examining the multi-target case in its entirety, consider a simpler load: a resistive load, R, with a series inductor, L, for filtering. Such a circuit could be used to model a single induction target. The load current's THD over a normalized fundamental output voltage range was also computed using MATLAB for both converters, with results shown in Fig. 12(b). In this plot, the THD of the full-bridge PWM inverter is shown again for three different frequency modulation ratios: M_f =3, 5, and 10. Unlike before, the distortion in the PWM case decreases noticeably in response to an increase in the frequency modulation ratio M_f. This is to be expected because increased modulation ratios move the switching harmonics to higher frequencies, making them easier to filter. In addition the distortion for a two-phase Marx inverter functioning as a seven-level symmetric uniform quantizer is also shown. Both the quantized Marx and PWM waveforms have fundamental frequencies at the $R/(2\pi L)$ frequency for the load. As shown in Fig. 12(b), the quantized waveform generally gives lower THD over the upper two-thirds of the achievable amplitude range even for the $M_f =$ 10 case. In fact over most of this range the percent THD is under 10%. Because the total delivered power is

$$P = (1 + \mathrm{THD}^2) I_{\mathrm{rms},1}^2 R \tag{11}$$

the THD is also useful for determining how much of the total power is the result of additional harmonics. For a percent THD under 10%, less than 1% of the delivered power is carried by the higher current harmonics. Note that below this amplitude range, only one level of the Marx converter is being exercised and therefore the amount of harmonic distortion grows rapidly.

In the previous, single target case, it was easy to see that for $M_f = 10$ the Marx output still gave lower THD, at least over a useful range of output voltages. Such conclusions are not as easy to draw in the case of multiple targets, where the THD in all loads must be considered simultaneously. Consider once more the multiple target system shown in Fig. 3. Recall that each target has a characteristic frequency determined by its self-inductance and resistance, and that the resistance from target to target varies by multiples of α. This scheme allows a target to heat preferentially when driven at its characteristic frequency. In order for this plan to be successful, any power delivered unintentionally through higher current harmonics must be minimized.

Consequently, in the case of the multitarget load, a useful measure of converter performance is how much the additional harmonics impact the relative heating of induction targets. The theoretical relative heating factor between consecutive targets for the sample case illustrated in Fig. 3 was calculated using MATLAB. This particular system had a separation factor $\alpha =$ 5, which implies a nominal relative heating factor of 2.6. The PWM switching frequency was set to three times the highest target frequency in order to produce the three plots shown in Fig. 13. This number avoids excessive PWM switching losses, yet is large enough to limit unwanted heating due to higher harmonics when driving the low and middle frequency induction targets. Fig. 13(a) shows the relative heating factor for the lowest frequency target when driven by both a quantized Marx waveform and a fast PWM waveform. In this case, the frequency modulation ratio with respect to target 1, denoted as $M_{f,1}$, is equal to 75. Because of the high switching frequency, PWM produces a superior sinewave, deviating only slightly for low fundamental voltage amplitudes. The quantized Marx waveform, which is made with significantly fewer switching transitions, still manages to stay within about 5% of the nominal heating factor for fundamental voltage amplitudes in the upper two-thirds range.

For the intermediate target, shown in Fig. 13(b) the frequency modulation ratio has been reduced by a factor of five to $M_{f,2} = 15$. At this switching frequency the PWM waveform only yields relative heating profiles that lie within 5% for fundamental voltages above $0.4V_{\mathrm{FB}}$. Over this range the quantized waveform is generally better. Lastly, Fig. 13(c) has a frequency modulation ratio of only, $M_{f,3} = 3$. It is interesting to note that when stimulating the highest frequency target, additional current harmonics actually increase the relative heating factor as opposed to decreasing this factor as seen in the lower frequency targets.

B. Comparing Converter Efficiencies

The unipolar PWM scheme is clearly capable of satisfying the THD requirements of the discussed multi-target induction heating system but must use a significant number of switching instances at high frequency to do so. A major limitation of this approach is that the converter will incur roughly the same switching losses for driving any target, even if it's the

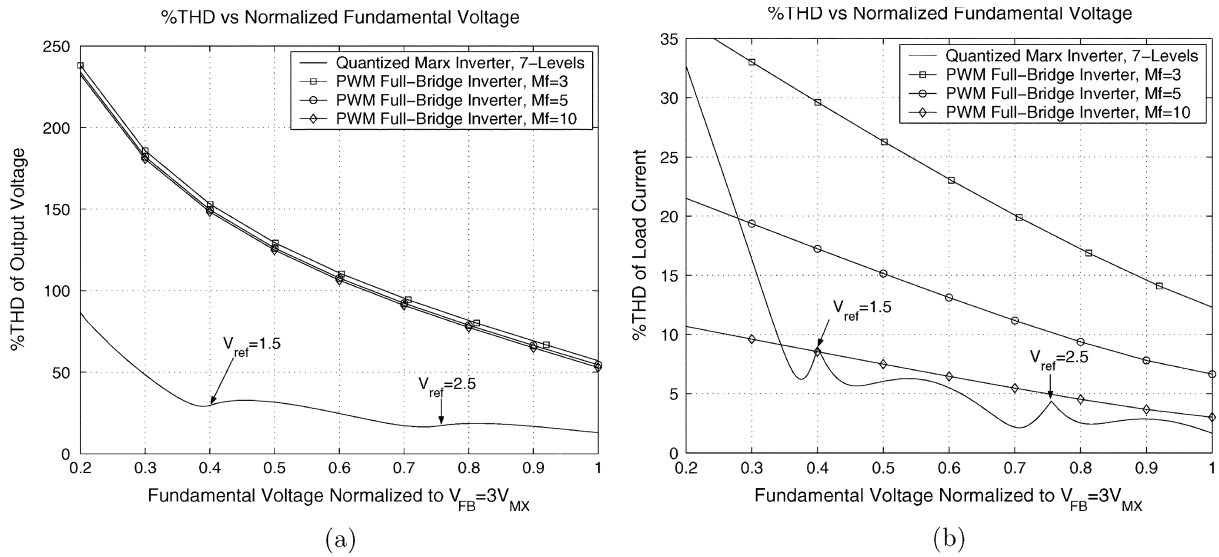

Fig. 12. Comparison of total harmonic distortion (THD) resulting from a sinusoidal PWM waveform versus a quantized sinewave: (a) THD of output voltage and (b) THD of current in the L–R load.

lowest frequency target. Furthermore, the magnitude of the switching losses are ultimately determined by the frequency of the highest frequency target, hence systems with greater than three targets or large separations in target frequencies can incur severe efficiency penalties. The Marx inverter circumvents these problems in two ways. First, the Marx converter runs at a switching frequency related to the frequency of the target being driven, not the frequency of the highest target. Second, the Marx inverter only needs to switch one-third as much voltage as the PWM full-bridge to achieve comparable power handling. The result is an additional reduction in switching losses for the Marx inverter relative to the full-bridge case.

For sinewave amplitudes in the range of $0.35V_{\rm FB}$ to $1V_{\rm FB}$, it was shown that a PWM inverter with a frequency modulation ratio of about three times the highest target drive frequency was needed to have comparable harmonic performance with a two-phase, seven-level Marx inverter. In order to have the same power capability, the full-bridge requires a bus voltage that is effectively three times the corresponding Marx inverter bus voltage, i.e., $V_{\rm FB} = 3V_{\rm MX}$. Having established the PWM switching frequency and the required bus voltage we are now in a position to compare the theoretical efficiencies of each converter. In order to simplify the comparison the following assumptions have been made.

- Layout parasitics are ignored, i.e., stray capacitance and interconnect resistance.
- The same switching device is used for both converters.
- All switching transitions are "hard."
- The load is inductive.

The efficiency of each converter was estimated by considering the following loss mechanisms.

1) Conduction losses.
2) Switching loss due to dissipatively charging and discharging the parasitic MOSFET output capacitance.
3) Switching loss due to non-zero turn-on and turn-off times.
4) Gate drive losses.
5) Losses due to capacitive voltage balancing (unique to the Marx converter).

A comparison of the first four losses are shown side-by-side for both the PWM full-bridge and a two-phase, seven-level Marx inverter (assuming all levels are used) in Table II. The losses associated with only using three or five levels are shown in Table III. The conduction loss of the Marx converter is worse, since the load current must traverse three times as many switches and up to an additional two ESRs associated with the Marx capacitors. As a result, the Marx inverter may not be an obvious choice when conduction losses dominate. However when switching losses dominate, the Marx inverter compares more favorably. The losses associated with charging and discharging the MOSFET output capacitance, $C_{\rm oss}$, are reduced by a factor of 6.75 (if $M_f = 3$). This assumes that $C_{\rm oss}$ is linear; if its nonlinearity is taken into account, the actual improvement will be less than 6.75.

The precise calculation of losses due to finite switching speeds requires knowledge of the exact load current value at each switching instant. Of the 16 active switching devices in the two-phase, seven-level Marx inverter, only twelve of them are used for switching the load current. Referring to Fig. 7, the remaining switches: $S_{1,\rm ph}$, $S_{2,\rm ph}$, $S_{4,\rm ph}$, and $S_{5,\rm ph}$ are only used for capacitor voltage balancing. Consequently, for our three target induction heating example, the number of switching instances (that commutate the load current) executed by the Marx inverter is at most equal to the number of switching instances of the PWM inverter when driving the highest frequency target ($M_f = 3$). At lower frequencies and voltages, the Marx inverter requires significantly fewer switch transitions to create an output waveform with THD comparable or superior to that of the PWM inverter. Even for the highest frequency, highest voltage case, when the number of switching instances for each converter is the same, the full-bridge is penalized by having to switch a voltage that is three times greater than that of the Marx inverter. In terms of the gate drive losses, the Marx converter is 33% higher when all seven levels are used—assuming the required gate charge is the same regardless of $V_{\rm ds}$ and $I_d(t)$. When only five of the levels are used the gate drive losses become equivalent. In practice, the charge required

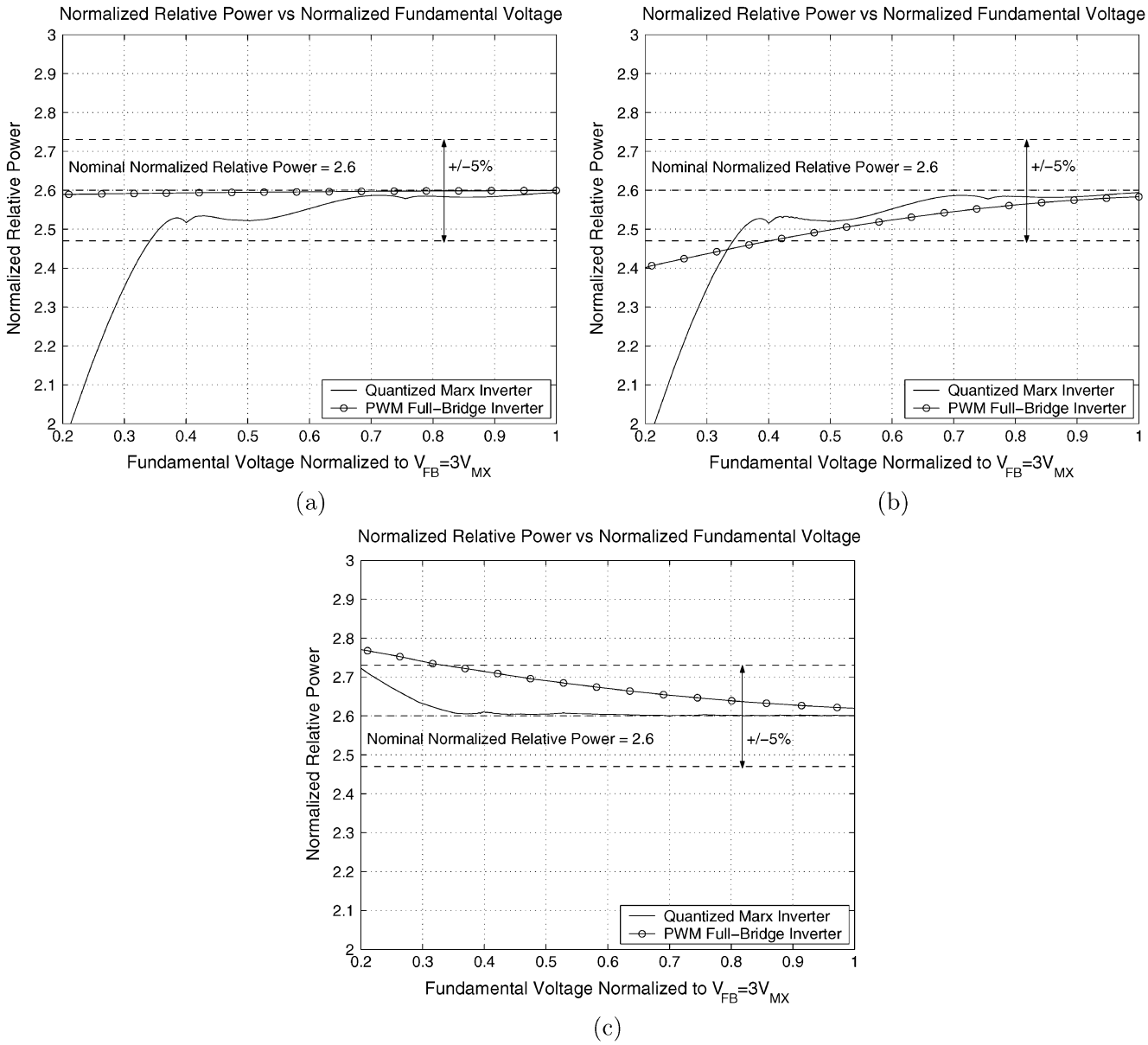

Fig. 13. Relative heating factor versus normalized fundamental voltage for the three target system depicted in Fig. 3 when excited by a PWM sinewave versus a quantized sinewave: (a) 4-kHz target, $M_{f,1} = 75$, (b) 20-kHz target, $M_{f,2} = 15$, and (c) 100-kHz target, $M_{f,3} = 3$.

for driving a MOSFET in the Marx inverter may be slightly lower because of the reduced bus voltage.

In general all switching loss mechanisms in the Marx inverter are reduced when less levels are needed, i.e., three levels or five levels. Perhaps more significant is the fact that losses decrease dramatically when we consider driving the intermediate and lowest frequency targets. In the lower frequency cases, the Marx inverter can operate at an effective switching frequency that is an additional factor of five or even 25 times lower than before, while the full-bridge cannot.

The Marx inverter does suffer from an additional loss mechanism not present in the full-bridge. Voltage balancing from capacitor to capacitor incurs dissipation. The conclusions reached in [8] concerning this phenomena also apply here. The energy lost is proportional to the voltage difference between capacitors squared and can be minimized by increasing the capacitance, C, or the switching frequency, f_s.

Using the simple expressions for these mechanisms the efficiency of each converter was calculated as a function of output voltage using MATLAB and then compared against actual data. For the purposes of testing and comparison each converter was built using International Rectifier's IRFB59N10D MOSFET. The efficiency for each converter was estimated assuming a series L–R load that gave a magnitude of 50 Ω with a phase angle of 45° at 100 kHz (the drive frequency). The computed MATLAB estimate along with actual measurements are shown in Fig. 14(a). The two lowest curves compare the full-bridge efficiency versus the Marx inverter for $V_{\mathrm{FB}} = 3V_{\mathrm{MX}} = 80$ V. As seen the loss equations predict that the Marx inverter is noticeably more efficient. The measured efficiencies support this even though it is clear that the estimates are somewhat conservative. This however is to be expected because the hand calculations assume that each switching instance is absolutely hard-switched. In truth this is not the case as the inductive load provides opportunities

TABLE II
COMPARISON OF LOSS MECHANISMS BETWEEN A PWM FULL-BRIDGE AND A TWO-PHASE, SEVEN-LEVEL MARX INVERTER FOR SINEWAVE GENERATION

Loss Mechanism	PWM (M_f=3, V_{ds}=V_{FB}=3V_{MX})	Marx (7 levels, V_{ds}=V_{MX})	Notes
Conduction Losses	$I^2_{rms}(2R_{ds,on})$	$I^2_{rms}(6R_{ds,on}+2R_{esr})$	1
MOSFET Output Capacitance	$4C_{oss,eff}(V_{ds})^2 M_f f_s$	$16C_{oss,eff}(V_{ds})^2 f_s$	2
t_{on} and t_{off} switching losses	$\frac{1}{2}[(V_{ds})(t_{on}+t_{off})f_s]$ $\times \sum_{t=1}^{4M_f} I_d(t)$	$\frac{1}{2}[(V_{ds})(t_{on}+t_{off})f_s]$ $\times \sum_{t=1}^{12} I_d(t)$	3
Gate Drive Losses	$4V_{cc}Q_g M_f f_s$	$16V_{cc}Q_g f_s$	4

TABLE III
MARX INVERTER LOSSES WHEN USING THREE OR FIVE (OUT OF SEVEN) LEVELS TO MAKE A QUANTIZED SINEWAVE

Loss Mechanism	Marx (3 levels, V_{ds}=V_{MX})	Marx (5 levels, V_{ds}=V_{MX})	Notes
Conduction Losses	$I^2_{rms}(6R_{ds,on}+2R_{esr})$	$I^2_{rms}(6R_{ds,on}+2R_{esr})$	1
MOSFET Output Capacitance	$6C_{oss,eff}(V_{ds})^2 f_s$	$12C_{oss,eff}(V_{ds})^2 f_s$	2
t_{on} and t_{off} switching losses	$\frac{1}{2}[(V_{ds})(t_{on}+t_{off})f_s]$ $\times \sum_{t=1}^{4} I_d(t)$	$\frac{1}{2}[(V_{ds}(t_{on}+t_{off})f_s]$ $\times \sum_{t=1}^{8} I_d(t)$	3
Gate Drive Losses	$6V_{cc}Q_g f_s$	$12V_{cc}Q_g f_s$	4

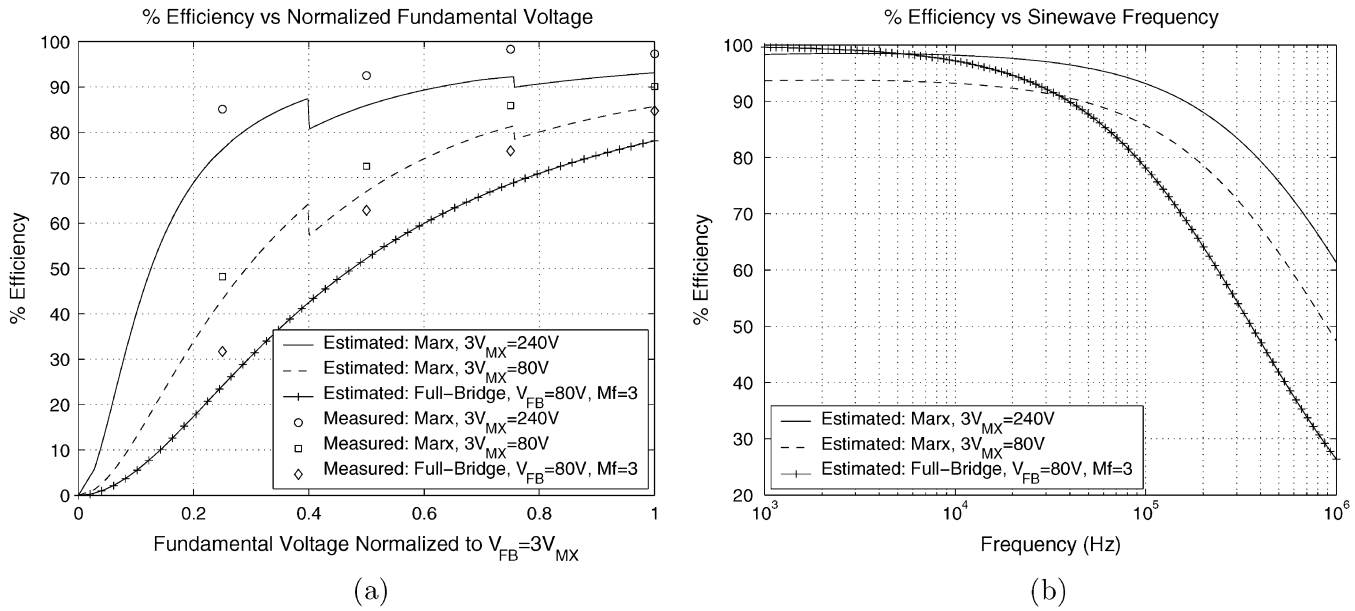

Fig. 14. Efficiency comparisons between a unipolar PWM full-bridge ($M_f = 3$) and a 2-phase, 7-level Marx inverter for sinewave generation. These comparisons use the same values of $t_{\rm on}$, $t_{\rm off}$, Q_g for each converter, ignoring the influence of $V_{\rm ds}$ and $I_d(t)$ on these parameters. $C_{\rm oss,eff}$ was calculated depending on the value of $V_{\rm ds}$. (a) Estimated and measured efficiency versus normalized fundamental voltage output. Sinewave frequency is 100 kHz and load impedance equals 50 Ω with a phase of 45 °. (b) Estimated efficiency as a function of sinewave frequency. The amplitude of the output sinewave equals $V_{\rm FB}$ or $3V_{\rm MX}$. Load impedance equals 50 Ω with a phase of 45 ° across all frequencies. This estimate ignores the ac resistance of $R_{\rm ds,on}$ and uses the value of $R_{\rm esr}$ at 100 kHz.

for at least half of the switching transitions to switch with less voltage as the inductor current discharges the MOSFET capacitance during the dead-time interval. Under proper loading and operating conditions the Marx inverter can generate sinewaves using zero voltage switching (ZVS). A discussion of these requirements can be found in [5].[1,2,3,4]

[1]Resistances associated with layout have been ignored.

[2]Because the MOSFET output capacitance is nonlinear it is useful to define an effectively linear capacitance, $C_{\rm oss,eff}$, such that $C_{oss,eff}V_{\rm ds}$ equals the amount of charge stored in $C_{\rm ds} + C_{\rm gd}$ for that value of $V_{\rm ds}$.

[3]This estimate is for a switching trajectory consistent with a diode clamped inductive load. The values for $t_{\rm on}$ and $t_{\rm off}$ may vary depending on the value of $V_{\rm ds}$ and $I_d(t)$.

[4]The required total gate charge, Q_g, is influenced by the value $V_{\rm ds}$ and $I_d(t)$.

The Marx bus voltage ($V_{\rm MX} = 26.666$ V) in this case was chosen merely for comparative purposes and represents an under utilization of the voltage blocking capability of the IRFB59N10D ($V_{\rm DSS} = 100$ V). If the bus voltage is increased three times this amount, the overall efficiency of the Marx inverter improves dramatically as shown by the top curve. Once again, the top curve represents a conservative figure. For the three normalized fundamental voltages above 0.5 the measured efficiencies were greater than 90%. Even when the normalized voltage amplitude was as low as 0.25 the efficiency was still about 85%.

Fig. 14(a) shows the efficiency of these converters at one particular frequency, 100 kHz. In a number of applications it is desirable to characterize the efficiency of these converters over

frequency. The loss expressions derived previously, can also be used for this purpose. A MATLAB script similar to the one that generated Fig. 14(a) was modified to calculate efficiency as a function of frequency assuming that the amplitude of the output sinewave equals V_{FB} or $3V_{\mathrm{MX}}$. For simplicity this particular script ignores the effects of frequency on conduction losses, i.e., ac resistance and variation of ESR in the Marx inverter's capacitors. For comparison purposes, the load used in this calculation has a magnitude of 50 Ω and a phase angle of 45° across all frequencies. The results of this analysis are shown in Fig. 14(b) for the same bus voltages that were examined in Fig. 14 (a). It was previously stated that the Marx inverter offers an improvement in efficiency when switching losses dominate. Using Fig. 14 (b) it is possible to infer at what frequency this occurs. In this particular case our loss equations predict that for frequencies greater than about 35 kHz the Marx inverter begins to offer comparably higher efficiencies as frequency is increased [14]–[17].

V. Conclusion

We are developing a tunable vibration damper that utilizes a thermally responsive gel material to reduce vibrations selectively in a frequency range. The tunable damper relies on the fact that a variable viscosity material can be used to alter the moment of inertia associated with a rotating auxiliary mass. This tuning mechanism can be used alone or in conjunction with other schemes, for example, adjusting the spring constant in the damper, to achieve variable frequency operation.

Thermal activation of each gel-filled compartment in the damper is accomplished using a noncontact induction heating scheme. Each chamber contains an induction target that is designed to exhibit preferential heating at a unique frequency. This multifrequency, multitarget approach can be used in numerous applications, including medical and industrial processes, to provide a wide range of spatial temperature control.

To properly induction heat any combination of these targets, a power supply capable of generating a sum of sinewaves is necessary. A reasonable degree of spectral purity is essential to ensure that unwanted harmonics do not cause undesired power loss in targets meant to be left unexcited. While a conventional PWM inverter could be used, the Marx inverter examined in this paper offers excellent, low harmonic distortion at high efficiencies.

References

[1] C. Harris and C. Crede, *Shock and Vibration Handbook (vol. 1)*. New York: McGraw-Hill, 1961.

[2] C. Ting-Kong, "Design of an Adaptive Dynamic Vibration Absorber," M.Eng. thesis, Univ. Adelaide, Adelaide, Australia, 1999.

[3] F. Forest, E. Laboure, F. Costa, and J. Gaspard, "Principle of a multiload/single converter system for low power induction heating," *IEEE Trans. Power Electron.*, vol. 15, no. 2, pp. 223–230, Mar. 2000.

[4] H. Haus and J. Melcher, *Electromagnetic Fields and Energy*. Englewood Cliffs, NJ: Prentice-Hall, 1989, pp. 446–447.

[5] J. Rodriguez, "A Multi-Frequency Induction Heating System for a Thermally Triggered Gel Polymer Dynamic Vibration Absorber," Ph.D. thesis, Mass. Inst. of Technol., Cambridge, 2003.

[6] J. Rodriguez, R. He, and S. Leeb, "Frequency selectable induction heating targets," in *Proc. Power Electron. Spec. Conf. (PESC)*, Acapulco, Mexico, Jun. 15–19, 2003, pp. 1943–1950.

[7] J. S. Lai and F. Z. Peng, "Multilevel converters—a new breed of power converters," *IEEE Trans. Ind. Appl.*, vol. 32, no. 3, pp. 509–517, May/Jun. 1996.

[8] F. Z. Peng, "A generalized multilevel inverter topology with self voltage balancing," *IEEE Trans. Ind. Appl.*, vol. 37, no. 2, pp. 611–618, Mar./Apr. 2001.

[9] J. Rodriguez, J. Lai, and F. Peng, "Multilevel inverters: A survey of topologies, controls, and applications," *IEEE Trans. Ind. Electron.*, vol. 49, no. 4, pp. 724–738, Aug. 2002.

[10] S. Sirisukprasert, J. Lai, and T. Liu, "Optimum harmonic reduction with a wide range of modulation indexes for multilevel converters," *IEEE Trans. Ind. Electron.*, vol. 49, no. 4, pp. 875–881, Aug. 2002.

[11] J. Rodriguez, L. Moran, P. Correa, and C. Silva, "A vector control technique for medium-voltage multilevel inverters," *IEEE Trans. Ind. Electron.*, vol. 49, no. 4, pp. 882–888, Aug. 2002.

[12] D. Holmes, "A general analytical method for determining the theoretical harmonic components of carrier based PWM strategies," in *Proc. Ind. Appl. Conf.*, Oct. 12–15, 1998, pp. 1207–1214.

[13] N. Mohan, T. Undeland, and W. Robbins, *Power Electronics Converter, Applications, and Design*. New York: Wiley, 1995.

[14] D. Jackson, "Inductively Coupled Power Transfer for Electromechanical Systems," Ph.D. thesis, Mass. Inst. of Technol., Cambridge, 1998.

[15] A. Nabae, I. Takahashi, and H. Akagi, "A new neutral-point-clamped inverter," *IEEE Trans. Ind. Appl.*, vol. IA-17, no. 5, pp. 518–523, Sep./Oct. 1981.

[16] L. Tolbert, F. Peng, and T. Habetler, "Multilevel converters for large electric drives," *IEEE Trans. Ind. Appl.*, vol. 35, no. 1, pp. 36–44, Jan./Feb. 1999.

[17] J. Chiasson, L. Tolbert, K. McKenzie, and Z. Du, "Eliminating harmonics in a multilevel converter using resultant theory," in *Proc. Power Electron. Spec. Conf. (PESC)*, Jun. 23–27, 2002, pp. 503–508.

John I. Rodriguez (S'02–M'04) received the S.B., M.Eng., and Ph.D. degrees in electrical engineering from the Massachusetts Institute of Technology (MIT), Cambridge, in 1997, 1999, and 2003 respectively.

While pursuing the degree of Ph.D. degree he was a Research Assistant in the MIT Laboratory for Electromagnetic and Electronic Systems (LEES). He is currently a Senior Scientist at Talking Lights, Brighton, MA. His research interests include power electronics, multilevel power conversion, induction heating, analog circuit design, and classical feedback control systems.

Steven B. Leeb (S'89–M'93–SM'01) received the S.B., S.M., E.E., and Ph.D. degrees from the Massachusetts Institute of Technology (MIT), Cambridge.

He has been a member of the MIT faculty in the Department of Electrical Engineering and Computer Science since 1993. He currently serves as a MacVicar Faculty Fellow and Professor of electrical engineering and computer science in the Laboratory for Electromagnetic and Electronic Systems. He is concerned with the design, analysis, development and maintenance process for all kinds of machinery with electrical actuators, sensors, or power-electronic drives.